Calculus Accumulation-based Method For Extracting Values Of Instrumentation Image

Dianming Wang[1*], Li Zhou[1], Xiangxin Chen[2], Mingxin Yi[2], and Xiaoju Yin[1]

[1] New Energy College, Shenyang Institute of Engineering, Shenyang 110136, China
[2] Liaoning Oriental Power Generation Co., Ltd.
[*] Corresponding author. E-mail: wm0231511@163.com

Received: Mar. 18, 2025; Accepted: Apr. 20, 2025

The working conditions of outdoor pointer instruments are complex, and the dial is vulnerable to environmental pollution, so it is difficult to identify the readings online accurately. A double-pointer meter reading recognition scheme based on two-dimensional convolution and calculus accumulation is proposed. The weighted multi-feature matching algorithm is used to accurately obtain the center coordinates of the rotating shaft to improve the success rate of meter image recognition. The template filtering method eliminates cross-pointer interference. The polar coordinate transformation and calculus accumulation of the dial image are carried out to obtain the position of the target double-pointer and realize automatic reading, which is suitable for most instruments. Through the experimental comparison and analysis of outdoor dust occlusion, droplet occlusion, leaf occlusion, and different lighting conditions, the results show that the algorithm has good robustness, is almost not disturbed by the external environment, and has high recognition accuracy. The recognition success rate is more than 98 %, which provides a good reference for the unattended operation of pointer instruments.

Keywords: Dual needle gauge recognition; Two dimensions convolution; Calculus accumulation; Two-axis coordinate system

http://dx.doi.org/10.6180/jase.202602_29(2).0002

1. Introduction

Pointer-type instrumentation anti-interference ability, good economy, and high reliability are widely used in power system generation, transmission, transformation, and distribution links [1]. Outdoor operation of pointer meters can not achieve communication interaction, manual inspection is time-consuming and laborious, and there are accuracy and subjectivity problems [2]. The use of robotic inspection to achieve visual recognition of pointer meters has become a hot research direction.

Many devices in the power system are equipped with dual-pointer instruments, such as oil temperature gauges, air pressure gauges, and transformer thermometers [3, 4]. Pointer meter reading is mainly based on image processing technology and deep learning methods. Deep learning algorithms have a high degree of automation [5, 6] and a large sample library, while computer vision methods run fast and are suitable for hardware-poor complex field applications [7, 8]. In recent years, research on pointer meter readings for outdoor operations has made some progress. Among these, extensive and in-depth research has been carried out both at home and abroad for the problem of uneven light that occurs in engineering applications. Li et al. [9] proposed a six-step preprocessing method for pointer meter images; Song et al. [10] proposed a Gaussian homomorphic high-pass filter; Zhang [11] designed an improved power-law transform function with a wide dynamic range, and Xing [12] used a correction algorithm based on a two-dimensional gamma function to reduce the impact of uneven illumination on the meter images. How-

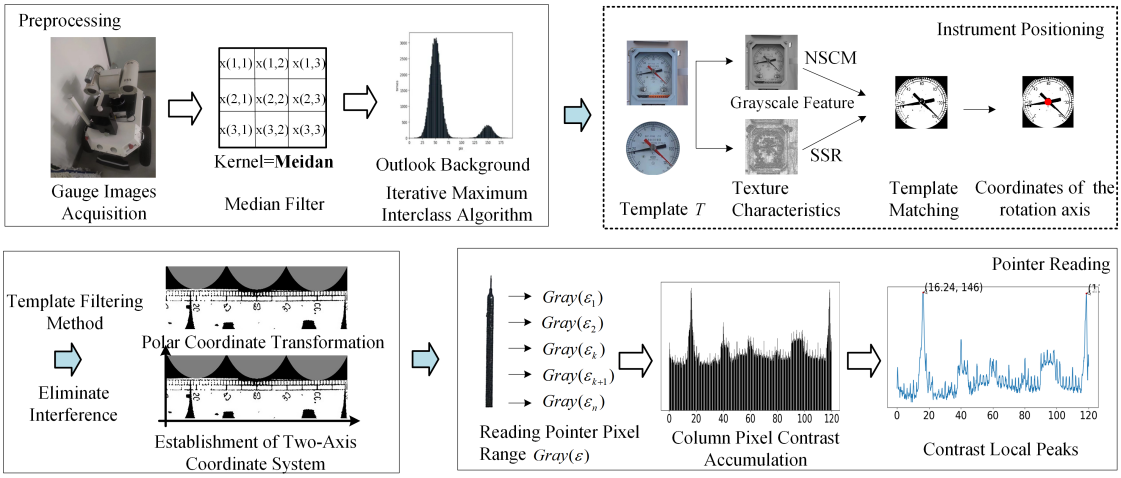

Fig. 1. Algorithm flowchart

ever, the dials of pointer meters operating outdoors are susceptible to environmental contamination, and a variety of occluders block effective key information. The robustness of the above algorithms to obstruction interference under real operating conditions is generally poor, making the application scenarios for outdoor robot detection very limited. For the study of dual-pointer meters, Sun et al. [13] proposed the target line segment filtering method, which determines the line segment filtering threshold with the help of auxiliary dial radius, eliminates the interference, and obtains the pointer line segments, which applies to the crossed dual-pointer meters. Li et al. [14] determine the position of dual pointers by Hough transform and geometric solution, which is suitable for concentric dual-pointer instruments. Xu et al. [15] extracted the image of a single-pointer meter based on the feature of the red color of the auxiliary dial pointer and scale and then carried out the reading detection. For dual-pointer meters operating under complex outdoor conditions, a recognition algorithm with stronger applicability is also needed.

Therefore, this paper proposes a target image recognition algorithm based on calculus accumulation and two-dimensional convolution, which can solve the problem of poor applicability of the above algorithms with high requirements on the appearance of meters, pointer shapes, scale densities, etc., with high robustness to obstacles, and is suitable for most pointer-type meters operating in outdoor environments, including dual-pointer meters. The specific contributions of the method are as follows:

1) A weighted multi-feature template matching algorithm is used for hierarchical matching, which improves the matching success rate and accurately locates the center coordinates of the rotation axis.

2) A calculus accumulation method under a dual-axis coordinate system is proposed, which transforms the line integration problem into a summation problem, saves computational power and can be deployed at the edge.

3) It is difficult for dust, light, and shadow interference to pass through the center of the pointer rotation axis and show a straight line similar to the pointer pixel value. Therefore, the calculus accumulation method has good robustness to masking and distortion.

4) A template filtering method is proposed to eliminate the cross-talk of double pointers, independent of meter-specific features, making calculus accumulation detection applicable to various types of double pointers.

2. Methods

2.1. Algorithm Design for Dual-Pointer Meter Reading

The two-dimensional convolution and calculus accumulation-based dual-pointer meter reading algorithm is shown in Fig. 1, which mainly consists of template configuration, image pre-processing, recognition region detection, pointer detection, and number of indications calculation.

(1) Template configuration. When using the power inspection robot high-speed camera to collect images, the preset shooting inclination should be as small as possible under the condition of meeting the terrain. Generally, the horizontal angle does not exceed 11°, and the vertical angle does not exceed 13°. To ensure detection speed and accuracy, the inspection robot's shooting position, azimuth, and elevation angle should be as consistent as possible. The dial area is archived as a standard image template before detection, and the pointer coordinates and cross-pointer angle are determined.

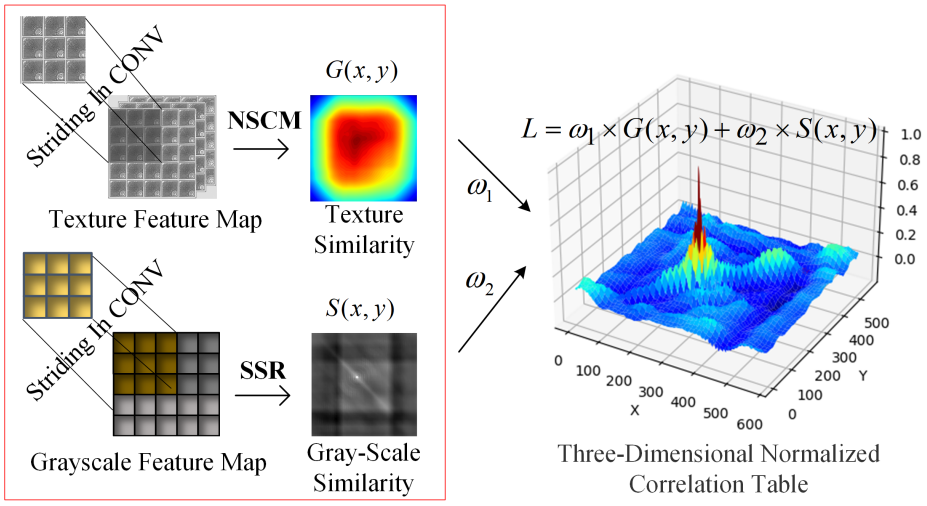

Fig. 2. Structure of weighted multi-feature template matching algorithm

(2) Image pre-processing. Median filtering was performed using a 5×5 template to suppress pretzel noise and reduce the blurring of image details [16]. Use the iterative maximum inter-class variance algorithm [17] to update the background after each segmentation to improve the image binarization results under poor lighting conditions.

(3) Recognition region detection. A weighted multi-feature template matching algorithm is proposed based on two-dimensional convolution to calculate the weighted similarity of greyscale and texture features, and the matching region is obtained by grading matching. According to the matching results and the coordinates of the pointer in the template, the coordinates of the rotation axis of the pointer in the matching region are found, which are used as the base point of the polar coordinate conversion of the instrument image.

(4) Pointer detection and calculation. The dial image is converted from the Cartesian coordinate system to the polar coordinate system, and a two-axis coordinate system is established according to the distribution of pixels. The polar coordinate image pixels and pointer pixels in the direction of the cumulative axis are matched, and the pointer position is at the cumulative maximum value, which is automatically read.

2.2. Weighted multi-feature template matching based on two-dimensional convolution

Accurate and rapid extraction of data under complex working conditions is an important part of the readout. A weighted multi-feature template matching method based on twodimensional convolution is proposed, and the structure of the algorithm is shown in Fig. 2. The Normalized Standard Correlation Matching (NSCM) algorithm calculates the grey scale similarity $G(x,y)$. Structural Similarity Ratio (SSR) is used to measure texture similarity $S(x,y)$, and the weights of greyscale and texture features are set according to different template conditions w_1/w_2. During the operation, the convolution kernel is aligned to each pixel point on the image, the dot product of the convolution kernel T and the corresponding sub-map is calculated according to Eqs. (1) and (2), and the weighted similarity result L is outputted to the corresponding pixel position to form a 3D normalized inter-relationship number table. Multiple discriminative criteria, such as pointer feature, contour, area, etc., are introduced to comprehensively evaluate the merits of the matching results.

Considering the complexity of practical application scenarios and improving accuracy, this algorithm uses hierarchical template matching. Set the instrument area according to the actual spacing of the inspection. The first level of matching acquires the instrument area, and the second level of matching sets the traversal area on the instrument area to locate the dial. For the auxiliary dial with a very small area, the third level of matching is carried out on the main dial. The normalized correlation matching algorithm normalizes the image to be detected and the template, and is robust to illumination. The structural similarity coefficient takes into account the texture information of the image and enhances robustness to slight rotations, scaling, and luminance changes. For circular meters, a circular mask is used to extract the matching region and reduce the subsequent calculus-accumulated interference terms.

$$G(x,y) = \frac{\sum_{x',y} \left(T'\left(x',y'\right) * I'\left(x+x',y+y'\right)\right)}{\sqrt{\sum_{x',y} \left(T'\left(x',y'\right)^2 * \sum'_{x',y'} \left(x+x',y+y'\right)^2\right)}} \quad (1)$$

$$S(x,y) = \frac{1}{N}\sum_{i=1}^{N}(T - T') * (I - I')$$
$$T = \sum_{n=0.7} g_n \times 2^n \tag{2}$$

$$L = w_1 \times G(x,y) + w_2 \times S(x,y) \tag{3}$$

Where: $T(x',y')$ is the mean grey value of the template; $I'(x+x', y+y')$ denotes the mean grey value of the image; * denotes the convolution operation. N is the number of neighborhood pixels; g_n denotes the local binarization result of the neighborhood pixel; T and I are the Local Binary Pattern(LBP) feature values of the template and the image, and T'/I' are the mean values of the LBP features of the template and the image, respectively.

The center of the rotation axis of the instrument determines the origin of the polar coordinate conversion, so the accuracy of the reading greatly depends on the accuracy of the extracted center [18, 19]. The existing center extraction method relies on the scale value information, and the robustness is poor when dealing with images of the instrument panel with obstructions, too bright, and too dark lighting. Using the coordinates of the pointer in the template and the coordinates of the template in the on-site image, the center P_0 of the rotation axis of the pointer can be found accurately, which is a low-complexity method and applies to all kinds of instruments.

2.3. Calculus Accumulation

2.4. Principle of Calculus Accumulation

The shape of the pointer is a closed curve; remember its greyscale image as a twodimensional image function $f(x,y)$. Radon transform is the image greyscale matrix to performs a fixed direction line integral, all the points of a straight line $L(\rho,\theta)$ in the XY plane are located at the same point in the AB plane. The straight line is detected according to the accumulated thickness g_i of each point on the AB plane.

$$g_i = \int_{Li} f(x,y)ds \tag{4}$$

The Radon transform geometry is shown in Fig. 3. Where ρ is the length along the line Li and θ is the identification angle of the direct Li. These two parameters establish that the straight line $L(\rho,\theta)\cdot\delta$ stands for the Dirac function.

$$L(\rho,\theta) = \{(x,y), \mathrm{x}\cos\theta + y\sin\theta = \rho\} \tag{5}$$

$$\int_L f(x,y)ds = \int_{-\infty}^{\infty}\int_{-\infty}^{\infty} f(x,y)\delta(x\cos\theta + y\sin\theta - \rho)dxdy \tag{6}$$

The straight line with a high grey value in the image $f(x,y)$ will form a bright spot in the AB space, while the line segment with a low grey value will form a dark spot in the AB space, and the sum can be used instead of the integral to simplify the computation at $\theta = 0$. It is easy to have local peaks when the Radon transform detects a straight line and does not get the desired results. However, based on the principle of line integration, a two-axis coordinate system is established, using target pixel points instead of projected intensities, and the function value at a point is a multiple of the sum of the target object's pixel points in the direction of this point's longitudinal coordinate, which is stable enough to obtain the global peak.

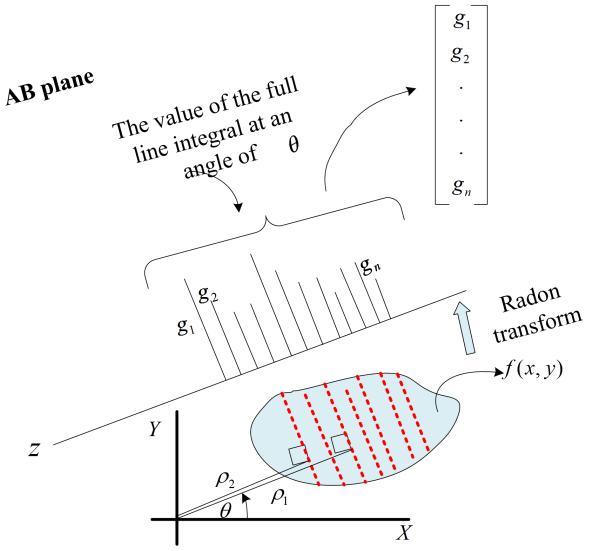

Fig. 3. Radon transform principle

2.5. Accumulation process

The two-axis coordinate system automatic reading effectively solves the problem of readings relying on scale and text information. Instrument images are processed using an erosion method that filters out the effects of environmental factors, pointer width, etc. on dial data. With reference to the distribution of pixel points, a two-axis coordinate system is established in the polar coordinate transformed image, with the direction parallel to the long axis of the pointer as the accumulation axis, and the other perpendicular direction as the movement calculation axis. Then, according to the target image algorithm flow of calculus accumulation, the sum of matched pixel points is calculated, and the corresponding maximum value position is the pointer position.

Remember the pointer grey scale range for Gray(ε), polar coordinate image grey scale value for Gray(x,y), when the initial position of the pixel grey scale value Gray$(x_0,y_0) \subset$ Gray(ε), the function value $f(x_0)$ plus 1, if different, then the function value f(x_0) plus 0. $x = x_0$ unchanged and $y+1$, repeat the judgment until the comple-

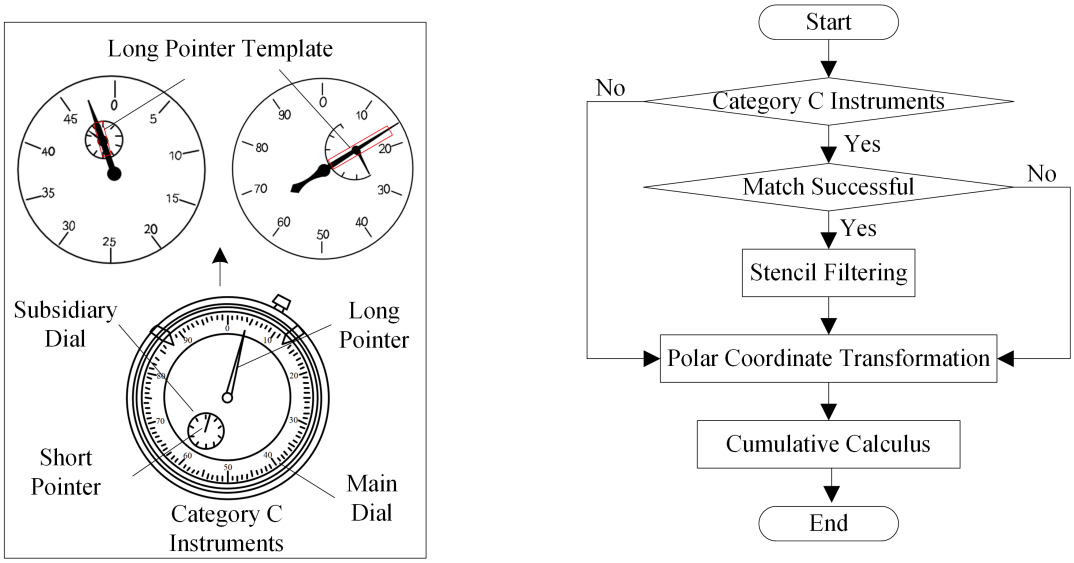

Fig. 4. Template-matched filtering method; left (a) Configuration templates; right (b) Flowchart

tion of the cumulative axis direction of the pixel matching, move the calculation axis coordinates plus 1, cumulative next pixel point until x also reached the boundary $\max(x)$, the cumulative completion. To facilitate reading, the 0 point of the moving calculation axis is overlapped with the starting position of the polar coordinate conversion image. After the overlap, the position of the target object located in the two-axis coordinate system can be quickly converted, and the coordinates can be intuitively read out in the calculus accumulation diagram to obtain the value automatically. Occlusions similar to pointer pixel values generally do not both pass through the center of the rotation axis and present a bar in the direction of accumulation, so the calculus accumulation method has good robustness.

2.6. Methods of reading different types of double-pointer type instruments

According to the positional relationship between the dial and the pointer, the existing dualpointer type instruments can be divided into 3 major categories. Category A instruments share a dial, but not necessarily a set of scale values. The pointers share the center of one axis of rotation and follow the calculus accumulation process to obtain the maximum two extreme values. The minimum accumulation threshold ratio is set, and there is only one polar point that satisfies the condition, indicating that the two pointers coincide. The two dials of the Category B meter are relatively independent, and the pointers do not cross, making them equivalent to two separate meters. The main dial of the class C instrument wraps the auxiliary dial, the long pointer and the short pointer may cross, and the long pointer has a very small probability of passing through the center of the rotation axis of the auxiliary dial, which interferes with the reading. However, the interference angle is fixed before the polar coordinate transformation, and using the template matching method to filter out the long pointer interference point, does not affect the reading.

As shown in Fig. 4, the template filtering method is divided into 2 steps.

1) Configure the template. The long pointer that passes through the center of the rotation axis of the auxiliary dial is used as a template, and the detected auxiliary dial is matched with the template, and the failure of template matching indicates that the long pointer has no interference with the auxiliary dial, so the polar coordinate transformation is carried out directly; and if the template matching succeeds, the long pointer will be filtered for the interference points.

2) Filter long pointer interference points. Create a mask image with a pixel value of 255, equal in size to the auxiliary dial image, which is eventually superimposed on the auxiliary dial image with the interfering pixel points removed. On the auxiliary dial, remove the matching pixel points using the matching center as the base point. Deleting the template long pointer minimum outer rectangle is recorded as Method 1, and splitting the outer fitting contour of the long pointer is recorded as Method 2. Comparing the two methods, the latter is slow and has poor robustness, and both of the calculus accumulation readings satisfy the accuracy requirements. As a result, the minimum outer rectangle elimination method is chosen to eliminate the dark pixels of the long pointer. Calculus

accumulation is carried out following the steps to obtain the auxiliary dial calculus accumulation curve, giving the readings.

3. Results and discussion

The Android system inspection robot is selected as the automatic inspection platform. It has a 5-core CPU, 8 GB of memory, a HIKVISION HD camera, with anti-collision radar, cruise control, and other related functions. PyCharm Community Edition is used as a software platform to process the instrument image.

To test the stability and applicability of the algorithm, 228 image samples of pointer gauges with different scales, different types, different weather environments, and different lighting conditions were collected at the actual test site, among which 120 images were normal operation images, 48 images were extreme lighting environments images, 24 images were dusty and soilobscured images, 24 water droplet-distorted images, and 12 images were leaf-obscured. The SQ-72 voltmeter is given for calculus cumulative curve analysis. The Transformer temperature indicator, MINGLE108 temperature, and humidity meter, 0-50 type Lugong per centimeter, Chuan system 01000101 per centimeter, are used for subsequent comparative experimental analysis. Instrument images are collected for the actual operating environment.

3.1. Matching results and processing

The traditional template matching algorithm is easily affected by a complex background, and the proportion of auxiliary dials is small, the clarity is low, and the matching accuracy is low. The weighted multi-feature template matching method can accurately locate the position of the dial in various instruments with uneven illumination distribution and different dial shapes, and the matching accuracy is increased from 52.3 % to 98.5 %. As shown in Fig. 5, the dial is finally extracted after two matches. A circular mask is used for the circular instrument to reduce subsequent text and background interference.

The accuracy of the polar coordinate transformation depends on the calculation accuracy of the center of the rotation axis. The traditional method fits the center of the curve by the connected domain where the scale is located and depends on the dial information. For the instrument image with a small radian range, clear scale, and strong connectivity, the connected domain fitting method can obtain a more accurate rotation axis center, while for the instrument image with a large radian range, blurred scale, and separated scale, the connected domain extraction effect is not good, and the polar coordinate transformation deviation

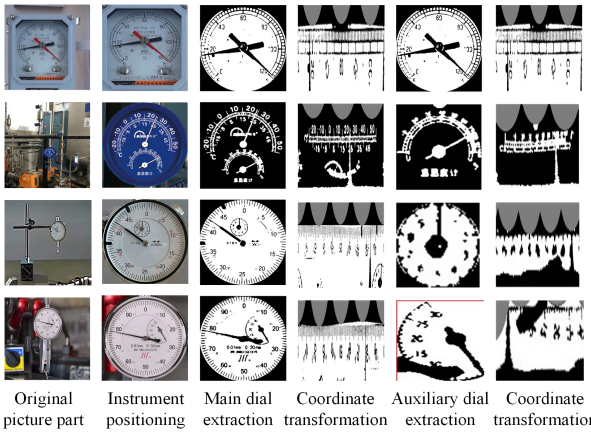

Fig. 5. Matching and transformation results

is great. This algorithm uses the pointer coordinates in the template and the template coordinates in the field image to accurately find the center of the pointer rotation axis, which is completely unaffected by the scale shape. The obtained polar coordinate conversion results are shown in Fig. 5, which is suitable for various instruments.

3.2. Analysis of the robustness of calculus accumulation to disturbances

The inspection robot reading recognition system is applied in the outdoor environment, which is affected by light, raindrops, dust, foliage cover, and other environmental influences, and it is difficult to extract relevant information such as scale line, pointer, etc., and the accuracy of pointer meter reading recognition is affected [20, 21]. The calculus accumulation recognition method is not subject to environmental interference, and has good anti-interference ability.

The non-polluted dashboard is set as the control group, and its calculus accumulation results have good regularity; the two-point peak advantage is obvious, higher than other local peaks 2-5 times. The SQ-72 Voltmeter head and tail of the main scale line are long, for the detection of the straight line algorithm caused more interference. However, it can not be closed to form an extreme point and does not interfere with the readings in this paper. In the leaf shading section of the simulation, the cumulative value rises significantly and the curve is deformed, but the dominant peak is still 1-3 times higher than the other values, and the results are within a reasonable range. When the droplet is above the dial information, affected by the refraction of the water droplet and the effect of light and shadow, the scale value and scale line information are distorted, which affects the result of calculus accumulation, and the curve shows non-regular fluctuation. By cutting the polar image processing,

Table 1. Algorithm comparison results

Simulation scenarios	Sample size	Accuracy ratio /%			Maximum quoted error /%			Average time /ms		
		Paper	[13]	[14]	Paper	[13]	[14]	Paper	[13]	[14]
Normal operation	120	**100**	93	90	**0.1**	2.2	2.3	557.3	550.4	**516.5**
Harsh lighting	48	**99**	82	81	**0.3**	5.4	4.8	551.1	569.7	**538.3**
Substantial obstruction	60	**98**	58	55	**0.3**	14.2	13.8	**547.2**	557.0	547.8

the influence caused by the interference is reduced, and the pointer advantage polar value is obvious, the waveform is stable, and the reading is accurate, as shown in Fig. 6.

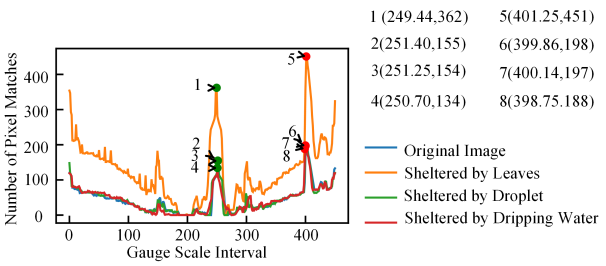

Fig. 6. Effect of foliage, droplet shading on calculus accumulation

The instrument image was obscured by dust condensation in the form of clumps, which affected the pointer pixel points during the image binarization and totalization process. The use of erosive imaging operations effectively reduces the effect of dust, and the calculus accumulation results show a small amount of irregular increase only at the large blocking, but the readings are still accurate. When the light intensity is poor, the use of the iterative Otsu algorithm can accurately segment the image, the calculus accumulation curve of the sample is consistent with the dial information law, the reading results are accurate, and have good robustness to light. As shown in Fig. 7, the calculus accumulation curves under extreme light and dust obscuration conditions are the same as under normal operating conditions, and the readings are accurate.

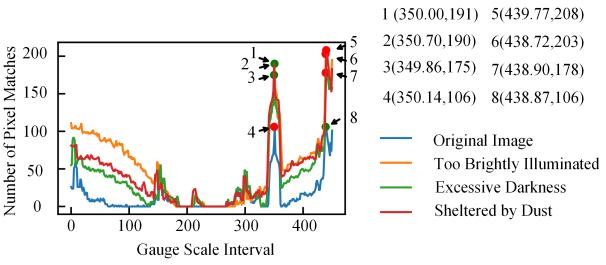

Fig. 7. Effect of dust and light variations on calculus accumulation

3.3. Pointer Reading Algorithm Results and Comparison

The average quoted error and maximum quoted error are introduced to evaluate the recognition accuracy and stability of various methods. x is the algorithmic reading, x_0 is the manual reading, x_m is the meter range. Then the quoted error γ_m is calculated by the formula:

$$\gamma_m = \frac{x - x_0}{x_m} \times 100\% \tag{7}$$

The maximum quoted error is the maximum value of the quoted error, and the average quoted error is the mean value of the quoted error.

Existing algorithms for dual pointer reading are based on a certain category of meter design. Sun et al. [13] applies to a percentage meter where the main dial contains a secondary dial, and a straight line is detected by using the target line segment separation filtering method together with the Hough transform Li et al. [14] applies to a temperature and humidity meter where the main and secondary dials are of different colors and the secondary dials are red, and the pointers and dials are detected by removing interferences, refining, Hough transform, and least squares method.

The main and auxiliary dials were manually separated to improve the applicability of the Sun et al. [13]. In the case of high occlusion, the recognition effect of the two reference methods is not good, especially for the auxiliary dial with less key information and difficult to detect, the failure probability of the reference method is large. Sun et al. [13], the target line segment separation filtering method filters the interference straight line by setting the threshold, and the proportion of the obstruction in the auxiliary dial is large, which affects the reading. The least squares method used in the Li et al. [14] is an algorithm that is not robust to interference, and the error of the Hough transform method originates from the continuity of the interfering straight lines by the obstructions, which leads to lower pixel accumulation values and non-straight line pixel misaccumulation during the voting process. For the 228 meter operation images captured for the actual scenario simulation, the results of the comparison of the three algorithms are shown in Table 1. In the table, paper represents the

methodology of this paper, and Sun et al. [13] and Li et al. [14] represents references [13, 14], respectively.

Using the instrument recognition algorithm to identify the experimental image, the correct recognition rate is more than 98%, the maximum quoted error is below 0.4%, and the single reading time is within 0.65 s , which meets the accuracy and real-time requirements of pointer reading detection, and the robustness is good for poor light and highly obstructed images, which is a method that can be adapted to the harsh production environment.

3.4. Cross-pointer-type instrument readings

Using the template matching method to traverse the auxiliary dial, find the long pointer's minimum outer rectangle, and exclude short pointer similar pixel points, the operation is rapid and simple. The original image calculus cumulative result has two similar interference peaks. After the template matching filtering method processing, the curve is read accurately. In addition, the larger extreme value is the accumulation of pixels at the tail of the short pointer, which does not constitute interference.

4. Conclusions

Aiming at the problem that the dial of pointer instrument for outdoor use is susceptible to the influence of light change, raindrop interference and dust obstruction, which leads to the problem that the scale line can not be extracted and the algorithm can not be read, a pointer instrument reading recognition method based on two-dimensional convolution and calculus cumulative is proposed, which applies to a variety of types of double-pointer instruments, and it mainly consists of three parts, namely, instrument area localization, pointer recognition and localization, and automatic reading. The method has the following features.

1) A weighted multi-feature template matching algorithm is proposed to set the weights of texture and grayscale features according to the a priori conditions of the meter, which improves the success rate of matching under the conditions of light change and angle change. Obtaining the pointer rotation axis center by template matching is more stable than other algorithms that rely on text and scale information to fit the rotation axis center, and is not disturbed by light and obstacles. The more accurate rotation axis center greatly eliminates errors such as tilt and distortion in polar coordinate conversion.

2) Aiming at the problem that the dial is distorted by a large number of water drops or obscured by dust under outdoor inspection conditions, a method is proposed to obtain the pointer position by calculating accumulation and automatically reading in the two-axis coordinate system. Polar coordinate transformation and morphological refinement operations reduce the interference of obstacles, and the property of calculus accumulation further reduces the influence of obstacles.

3) The calculus accumulation method has good robustness to the two-pointer crossinterference, and for the very few images in which the long pointer crosses the center of the rotation axis of the auxiliary dial, the template matching filtering method is proposed to exclude the interference of the main pointer against the effective pixel points, which is simple and effective, and has a good value for practical application.

5. Acknowledgments

This research was sponsored in part by the Project of Liaoning Provincial Department of Education in 2022 (LJKMZ20221728), the 2023 Liaoning Province Science and Technology Plan Joint Plan (2023JH2/101700253), and the 2023 Liaoning Provincial Department of Education Project (JYTQN2023092).

References

[1] Y. Liu, F. Wang, and Y. Zhang, (2025) *"Dual-plane Center-based Secondary Calibration Algorithm for Pointer-type Instruments"* **Instrument Technique and Sensor *000***: 32–38, 50. DOI: 10.3969/j.issn.1002-1841.2025.01.006.

[2] D. Peng, M. Huang, E. Qi, J. Hu, and X. Yang, (2023) *"Pointer Gauge Recognition Method of Thermal Power Plant Based on Yolov4"* **Computer Applications and Software *040***: 166–172, 222. DOI: 10.3969/j.issn.1000-386x.2023.06.026.

[3] B. Cheng, W. Zhu, R. Cheng, and R. Huang, (2025) *"Dual Pointer Industrial Meter Reading Recognition Based on Image Segmentation and Centre of Mass Fitting Method"* **Journal of Image and Signal Processing *014***: 12–20. DOI: 10.12677/jisp.2025.141002.

[4] Y. Mao, G. Yu, Q. Guo, and J. Liu, (2025) *"Survey of Image Detection and Recognition Methods for Pointer Meter"* **Automation & Instrumentation *040***: 6–9, 38. DOI: 10.19557/j.cnki.1001-9944.2025.02.002.

[5] Q. Sun, S. Liu, D. Liu, X. Song, J. Liu, and R. Liu, (2025) *"Few-shot pointer meters detection method based on meta-learning"* **Journal of Graphics *046***: 81–93. DOI: 10.11996/JG.j.2095-302X.2025010081.

[6] S. Li, L. Hou, and Y. Dong, (2024) *"Automatic reading of pointer meters based on R-YOLOv7 and MIMO-CTFNet"* **Journal of Graphics *045***: 1313–1327. DOI: 10.11996/JG.j.2095-302X.2024061313.

[7] Y. Pan, Y. Yao, L. Zhang, and J. Gao, (2024) *"Reading Recognition Method for Pointe Meters Based on Irregula Object Detection"* **Instrument Technique and Sensor *000***: 100–105. DOI: 10.3969/j.issn.1002-1841.2024.06.017.

[8] Z. Zuo, Y. Li, L. Chen, and X. Xie, (2024) *"Method Research on Automatic Reading of Pointer Instrument Based on Machine Vision"* **Instrument Technique and Sensor *000***: 37–40. DOI: 10.3969/j.issn.1002-1841.2024.06.007.

[9] X. Li, R. Wang, S. Tang, and J. Ming, (2012) *"Six-step pretreatment for image of pointer instrument"* **Electrical Measurement & Instrumentation *49***(12): 28–31. DOI: 10.3969/j.issn.1001-1390.2012.12.006.

[10] W. Song, W. Zhang, J. Zhang, Y. Wang, Q. Zhou, and W. Shi, (2014) *"Instrument reading recognition method via the pointer region feature"* **Chinese Journal of Scientific Instrument *35***(S2): 50–58. DOI: 10.19650/j.cnki.cjsi.2014.s2.008.

[11] W. Zhang. *"Research on instrument reading recognition algorithm for mobile robot outdoor inspection"*. (mathesis). Harbin Institute of Technology, 2022. DOI: 10.27061/d.cnki.ghgdu.2022.004440.

[12] Z. Xing. *"Research on detection and identification method of pointer instrument in substation environment"*. (mathesis). Anhui University of Science and Technology, 2021. DOI: 10.26918/d.cnki.ghngc.2021.000652.

[13] Y. Sun, W. Li, Y. Zhao, L. Ren, and W. Jiang. "A method for image recognition of intersectant dual-pointer instrument". In: *XXIII IMEKO World Congress Proceedings: Measurement: sparking tomorrow s smart revolution.Yokohama, Japan.30 August - 03 September 2021*. 2021. DOI: 10.1016/j.measen.2021.100224.

[14] Z. Li, Y. Sun, W. Hu, and X. Li, (2016) *"A method for automatic recognition of dual pointer instrument reading based on digital image process technology"* **Journal of Yangtze University (Natural Science Edition) *13***(31): 31–36+4. DOI: 10.16772/j.cnki.1673-1409.2016.31.007.

[15] Z. Xu, H. Yang, L. Liu, D. Wang, and L. Yu, (2019) *"Recognition scheme for point-er type temperature and humidity instrument based on image processing"* **Foreign Electronic Measurement Technology *38***(07): 32–36. DOI: 10.19652/j.cnki.femt.1901440.

[16] L. Li, Y. Qiao, X. Huang, W. Xie, and W. Jiang, (2025) *"Pointer meter reading recognition method based on improved U2-Net"* **Modern Electronics Technique *048***: DOI: 10.16652/j.issn.1004-373x.2025.05.026.

[17] Z. Ren and Z. Cao, (2024) *"Pointer Meter Reading Algorithm Based on Improved GA-Otsu and RANSAC Regression"* **Machine Design & Research *040***: DOI: 10.13952/j.cnki.jofmdr.2024.0080.

[18] Y. Qian, Z. Wang, and T. Qiu, (2024) *"Research status and development of pointer meter reading recognition"* **Electronic Measurement Technology *047***: DOI: 10.19651/j.cnki.emt.2415631.

[19] Z. Xia, W. Li, and Z. Tian, (2023) *"Research on Automatic Reading Method of Pointer Meter Based on YOLOv5"* **Instrument Technique and Sensor *000***: DOI: 10.3969/j.issn.1002-1841.2023.06.008.

[20] M. Liu, B. Wang, P. Luo, F. Ma, Y. Zhang, and L. Wang, (2024) *"Research on Pointer Meter Recognition Algorithm of Outdoor Inspection Robots"* **High Voltage Engineering *050***: DOI: 10.13336/j.1003-6520.hve.20231408.

[21] J. Zhang, L. Zeng, T. Liu, L. Deng, Z. Xu, and Z. Chen, (2023) *"Automatic reading algorithm of pointer instrument based on machine vision"* **Instrument Technique and Sensor *000***: DOI: 10.3969/j.issn.1002-1841.2023.11.010.